Supporting Information

Unraveling Non-Radiative Decay Channels of Exciplexes to Construct Efficient Red Emitters for Organic Light-Emitting Diodes

Heng-Yuan Zhang, Ming Zhang, Hao Zhuo, Hao-Yu Yang, Bo Han, Yong-Hao Zheng, Hui Wang, Hui Lin, Si-Lu Tao, Cai-Jun Zheng,* and Xiao-Hong Zhang**

Table of contents

Experimental section

General Information. The ^{1}H and ^{13}C NMR spectra were recorded via an Agilent DD2 400-MR spectrometer at room temperature. Mass spectra were obtained with a Shimadzu Biotech Axima Confidence high-resolution mass spectrometer. Crystals of SAF-2NP and mPTBC were grown by slow evaporation of the mixture of dichloromethane and n-hexane. The single crystal of TPh-2NP was grown by slow evaporation of Trichloromethane. Data were collected from a shock-cooled single crystal at 150 K on a Bruker D8 VENTURE dual wavelength Cu three-circle diffractometer with a microfocus sealed X-ray tube using a mirror optics as monochromator and a Bruker PHOTON III detector. The structures were solved by direct methods using SHELXT and refined by full-matrix least-squares methods against F^2 by SHELXL-2019/1. Electrochemical analysis was carried out using a CHI600E electrochemical analyzer. Thermogravimetry-differential scanning calorimetry (TG-DSC) was conducted using NETZSCH STA 449F5 at heating speed of 10 K/min. N,N-Dimethylformamide was used for reduction potential test and dichloromethane for oxidation potential test. The solution was degassed with N_2 for 10 min before the test. Tetrabutylammonium hexafluorophosphate were the supporting electrolyte. Two platinum disks and an Ag electrode were respectively employed as the working/counter and reference electrodes with standardized against ferrocenium/ferrocene (Fe$^+$/Fe). The cyclic voltammetry (CV) was recorded at a rate of 0.1 V s^{-1}. The UV-visible absorption spectra were measured with a Shimazu UV-2600 spectrophotometer and the photoluminescence spectra were recorded on a Hitachi F-4600 fluorescence spectrometer. FT-IR spectra were recorded using Thermofisher Nicolet 6700. Transient photoluminescence decay spectra were obtained with Horiba Single Photon Counting Controller: FluoroHub and Horiba TBX Picosecond Photon Detection. The prompt component was measured using a 370 nm NanoLED and a 370 nm SpectraLED was used in delayed fluorescence measurement. The absolute PL quantum yields were recorded on a Hamamatsu C9920-02G spectrometer. All doped films were prepared through vapor deposition.

Device fabrication. Indium tin oxide (ITO) glass substrates with a sheet resistance of 15 Ω per square were firstly cleaned with acetone, ethanol, and deionized water, and then dried in an oven at 120 °C for 2 h. Prior to being put into the thermal deposition instrument, the substrates were treated with UV-ozone for 20 minutes. Under a pressure below 5×10^{-4} Pa, the organic layers were deposited at a rate of 0.10-0.12 nm s^{-1} onto the ITO substrate sequentially. Onto the electron transporting layer, 1 nm LiF was deposited at a rate of 0.1 nm s^{-1} to improve electron injection. Finally, a 100-nm-thick layer of Al was deposited at a rate of 1 nm s^{-1} as

the cathode. The optical and electrical data of the devices were obtained with a PR655 Spectrscan and Keithley 2400 Source Meter under ambient atmosphere simultaneously. The current efficiencies, power efficiencies, and external quantum efficiencies were calculated with the data of current, luminance, and emission, assuming a Lambertian distribution.

Computational methods. Density functional theory (DFT) and time-dependent density functional theory (TD-DFT) simulations were performed Gaussian 16 A.03 program package. Optimized S_0, S_1 and T_1 structures of SAF-2NP, TPA-2NP, TPA-QP, mPTBC and mPTZC were calculated at the B3LYP/6-31G(d) level. Root-mean-square displacements (RMSD) were calculated according to RMSD =

$$\sqrt{\frac{1}{N}\sum_{i=1}^{N}[(x_i - x'_i)^2 + (y_i - y'_i)^2 + (z_i - z'_i)^2]}$$

, where N is the total atom number of the whole molecule (including hydrogen). (x_i, y_i, z_i) and (x'_i, y'_i, z'_i) denote the atom coordinates based on different geometries. Huang-Rhys factors and reorganization energy were calculated using the DUSHIN program according to frequency calculation by Gaussian. The atomic charges were fitted using the Merz-Kollmann method. Geometries of the bicomponent groups were optimized under B3LYP-D3(BJ)/6-31G(d) level. Theoretical visualization of hydrogen bonding was realized using the IGMH method in Multiwfn. The interaction energy was calculated under B3LYP-D3(BJ)/6-31G+(d,p) considering the basis set superposition error (BSSE).

Analysis of Rate Constants

Rate constants were calculated according to:[1]

$$k_{\mathrm{d}} = \frac{1}{\tau_{\mathrm{d}}}$$

$$k_{\mathrm{p}} = \frac{1}{\tau_{\mathrm{p}}}$$

$$k_{\mathrm{RISC}} = \frac{k_{\mathrm{p}}+k_{\mathrm{d}}}{2} - \sqrt{\left(\frac{k_{\mathrm{p}}+k_{\mathrm{d}}}{2}\right)^2 - k_{\mathrm{p}}k_{\mathrm{d}}\left(1+\frac{\Phi_{\mathrm{d}}}{\Phi_{\mathrm{p}}}\right)}$$

$$k_{\mathrm{f}} = \frac{k_{\mathrm{p}}k_{\mathrm{d}}}{k_{\mathrm{RISC}}}\Phi_{\mathrm{PL}}$$

$$k_{\mathrm{nr}} = \frac{k_{\mathrm{p}}k_{\mathrm{d}}}{k_{\mathrm{RISC}}}\left(1-\Phi_{\mathrm{PL}}\right)$$

Where k_{p} and k_{d} are the decay rate constants for prompt and delayed fluorescence, respectively; τ_{p} and τ_{d} are the prompt fluorescence lifetime and delayed fluorescence lifetime, respectively; Φ_{PL}, Φ_{p} and Φ_{d} respectively represent the total, prompt and delayed fluorescence quantum efficiency; k_{RISC}, k_{f} and k_{nr} are the rate constants of RISC, fluorescence decay and non-radiative decay of singlet excitons, respectively.

Synthesis and thermal stability
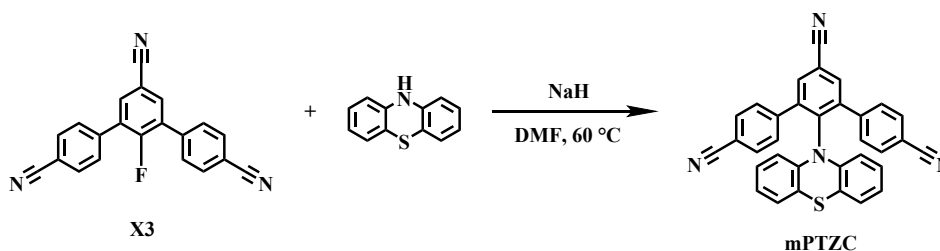
**Synthesis of 2'-(10H-phenothiazin-10-yl)-[1,1':3',1''-terphenyl]-4,4'',5'-tricarbonitrile (mPTZC).** The intermediate X3 was synthesized according to our previous report.[2] Phenothiazine (1.00g, 5.0 mmol) was degassed and dissolved in 20 ml dry DMF. The mixture was cooled to 0 °C and added to NaH (0.24 g, 10.0 mmol) in a 100 mL double-necked flask dropwise at 0 °C under nitrogen. X3 (1.29g, 4.0 mmol) was added afterwards and the reaction was stirred at room temperature for 0.5 h and then heated up to 60 °C and stirred for 4 hours. Brine and dichloromethane were added for extraction subsequent to the reaction was quenched by water. The organic layer was dried with anhydrous magnesium sulfate. After being concentrated by rotary evaporation, the residual solid was purified by column chromatography and recrystallization to give a bright yellow powder (1.12 g, yield 56%). ^{1}H NMR (400 MHz, Chloroform-d) δ 7.91 (d, J = 1.2 Hz, 2H), 7.60 (dd, J = 8.3, 1.7 Hz, 4H), 7.39 (dd, J = 8.4, 1.7 Hz, 4H), 6.63 (s, 6H), 5.80 (d, J = 7.6 Hz, 2H). ^{13}C NMR (101 MHz, Chloroform-d) δ 144.20, 140.86, 139.84, 135.63, 132.42, 129.14, 126.62, 126.48, 123.08, 118.21, 118.06, 117.06, 114.84, 113.95, 112.71. MALDI-TOF-MS [M]$^-$: calculated for $C_{33}H_{18}N_4S$: 502.1252, found: 502.0864.
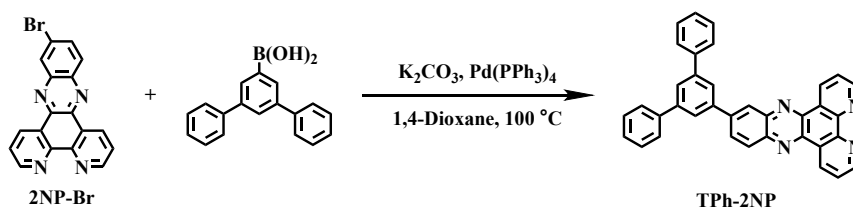
**Synthesis of 11-([1,1':3',1''-terphenyl]-5'-yl)dipyrido[3,2-a:2',3'-c]phenazine (TPh-2NP).** The intermediate 2NP-Br was synthesized according to our previous report.[3] A mixture of 2NP-Br (722 mg, 2.0 mmol), [1,1':3',1''-terphenyl]-5'-ylboronic acid (603 mg, 2.2 mmol) was dissolved in 20 mL 1,4-dioxane in a 100 mL double-necked flask. Afterwards, tetrakis(triphenylphosphine)palladium (0.24 g, 0.2 mmol) and K2CO3 (5 ml, 2 M) were added under nitrogen. The reaction was heated to 100 °C and stirred for 12 hours. After cooling to room temperature, the mixture was extracted with dichloromethane and water and dried over anhydrous magnesium sulfate. After being concentrated by rotary evaporation, the residual solid was purified

by column chromatography and recrystallisation to give a light green powder (796 mg, yield 79%). ^{1}H NMR (400 MHz, Chloroform-*d*) δ 9.61 (dt, *J* = 8.1, 1.5 Hz, 2H), 9.28 (dd, *J* = 4.5, 1.6 Hz, 2H), 8.63 (t, *J* = 1.5 Hz, 1H), 8.41 (d, *J* = 8.8 Hz, 1H), 8.29 (dt, *J* = 8.9, 1.6 Hz, 1H), 8.03 (d, *J* = 1.5 Hz, 2H), 7.91 (t, *J* = 1.6 Hz, 1H), 7.77 (ddd, *J* = 8.3, 3.9, 2.6 Hz, 6H), 7.57 – 7.48 (m, 4H), 7.48 – 7.39 (m, 2H). ^{13}C NMR (101 MHz, Chloroform-*d*) δ 152.46, 152.38, 143.19, 142.81, 142.63, 141.93, 141.46, 140.90, 140.74, 140.48, 133.84, 130.63, 129.92, 128.93, 127.79, 127.61, 127.54, 127.34, 126.82, 126.29, 125.42, 124.17. MALDI-TOF-MS: [M+H]$^-$: calculated for $C_{36}H_{22}N_4$: 511.1928, found: 511.1543.
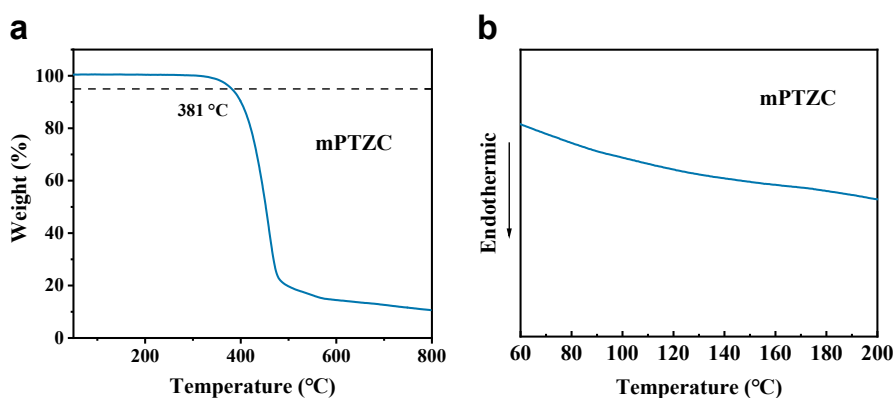
Figure S1. (a) TGA and (b) DSC curves of mPTZC.

Steady-state PL spectra and electrochemical measurements
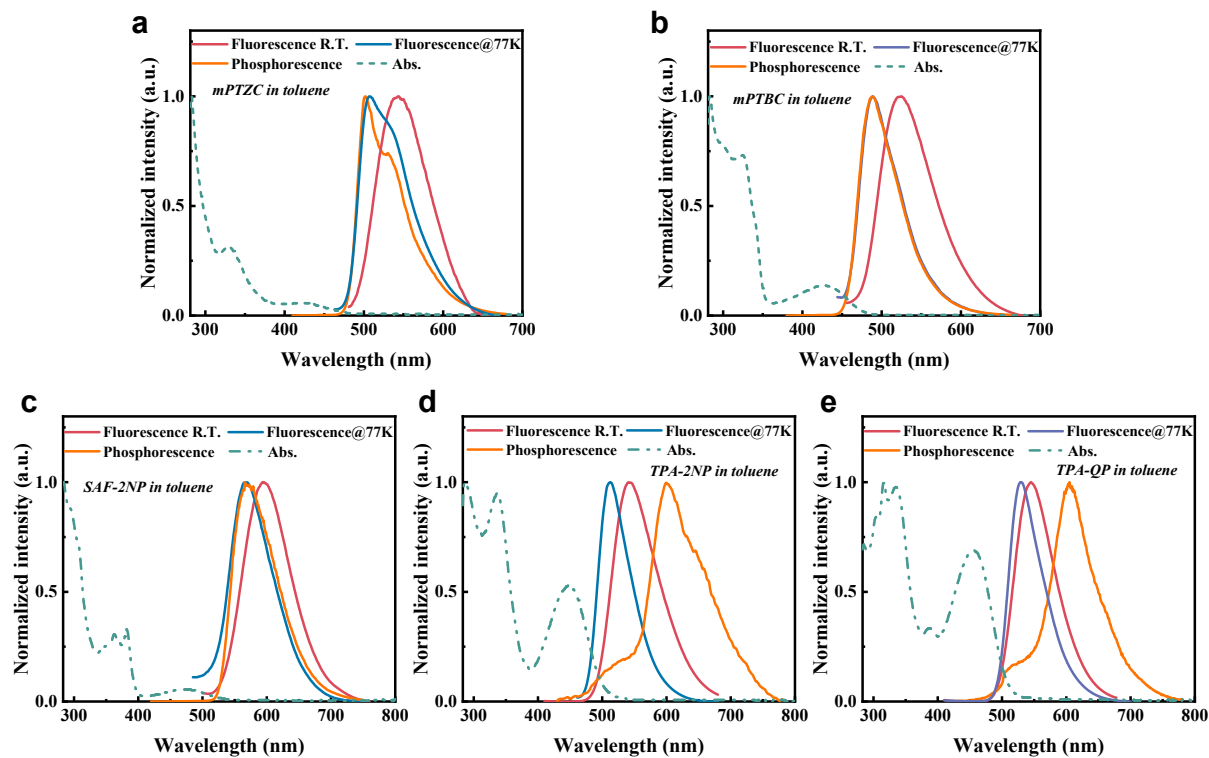
Figure S2. Normalized absorption, fluorescence and phosphorescence spectra of donors and acceptors measured in dilute toluene.
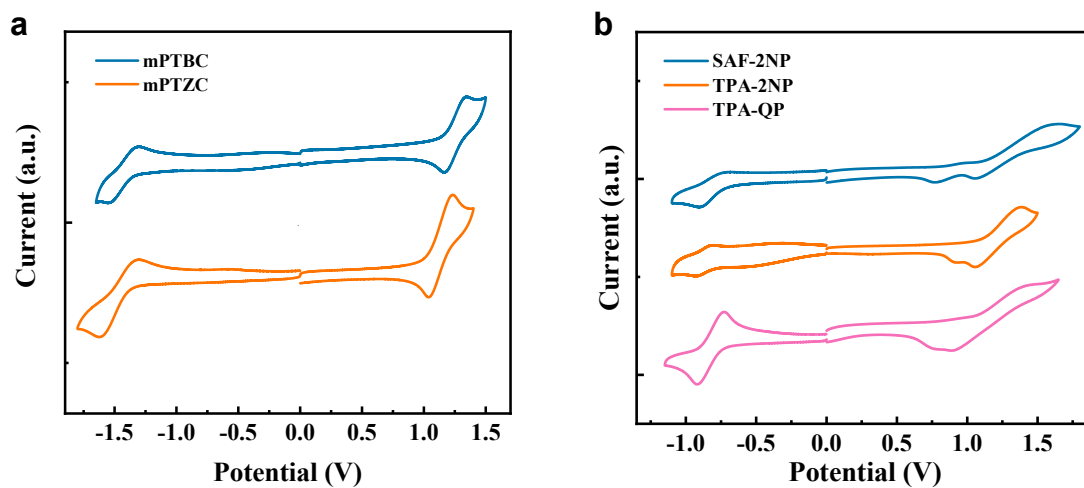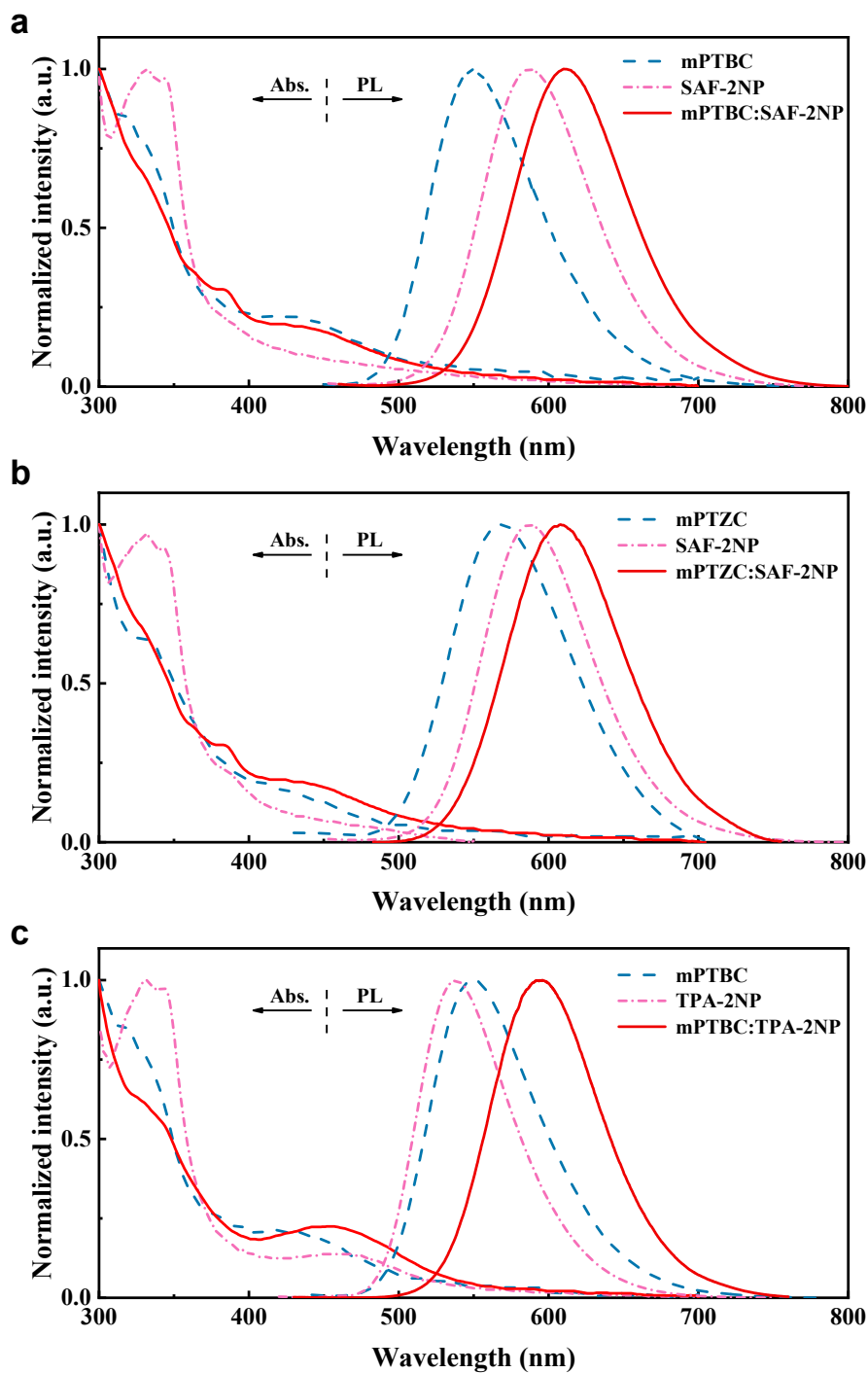

Figure S3. Oxidation and reduction curves of a) mPTBC, mPTZC and b) SAF-2NP, TPA-2NP, TPA-QP.

Table S1. Key physical properties of the two donors and three acceptors

Emitter	λ_{PL} (nm)	S_1 (eV)	T_1 (eV)	ΔE_{ST} (eV)	HOMO (eV)	LUMO (eV)
mPTBC	525	2.72	2.71	0.01	-5.21	-2.69
mPTZC	543	2.59	2.58	0.01	-5.07	-2.66
SAF-2NP	595	2.38	2.35	0.03	-5.39	-3.32
TPA-2NP	541	2.59	2.26	0.33	-5.36	-3.27
TPA-QP	545	2.51	2.28	0.23	-5.30	-3.31

Figure S4. Solid-state normalized absorption and photoluminescence spectra of exciplexes and corresponding constituents. a) mPTBC:SAF-2NP. b) mPTZC:SAF-2NP. c) mPTBC:TPA-2NP. Donor:acceptor = 9:1 (weight ratio). The spectra of SAF-2NP and TPA-2NP are measured with doping concentration of 10 wt% in CBP.
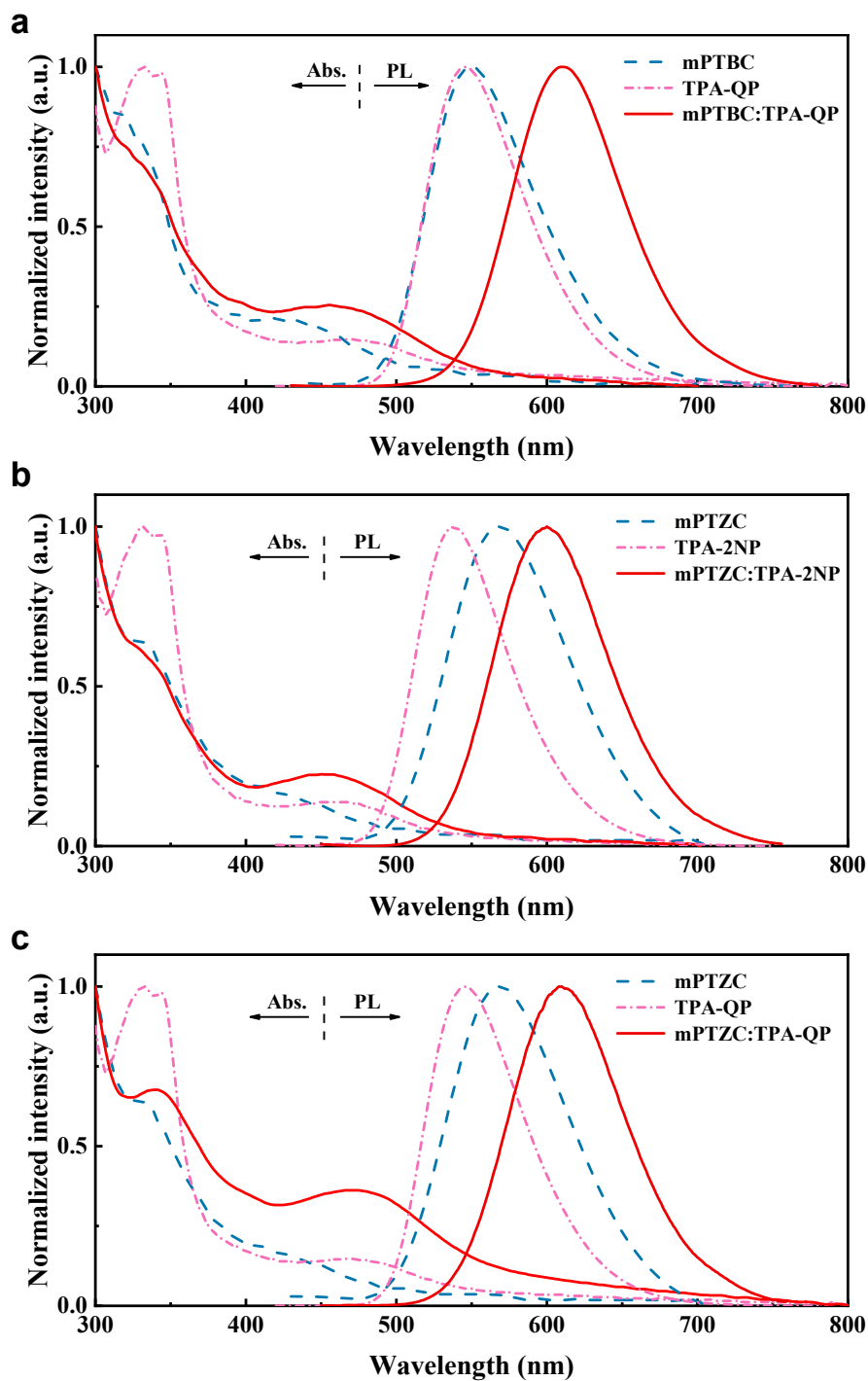
Figure S5. Solid-state normalized absorption and photoluminescence spectra of exciplexes and corresponding constituents. a) mPTBC:TPA-QP. b) mPTZC:TPA-2NP. c) mPTZC:TPA-QP. Donor:acceptor = 9:1 (weight ratio). The spectra of TPA-2NP and TPA-QP are measured with doping concentration of 10% in CBP.

Theoretical calculation and FT-IR spectra
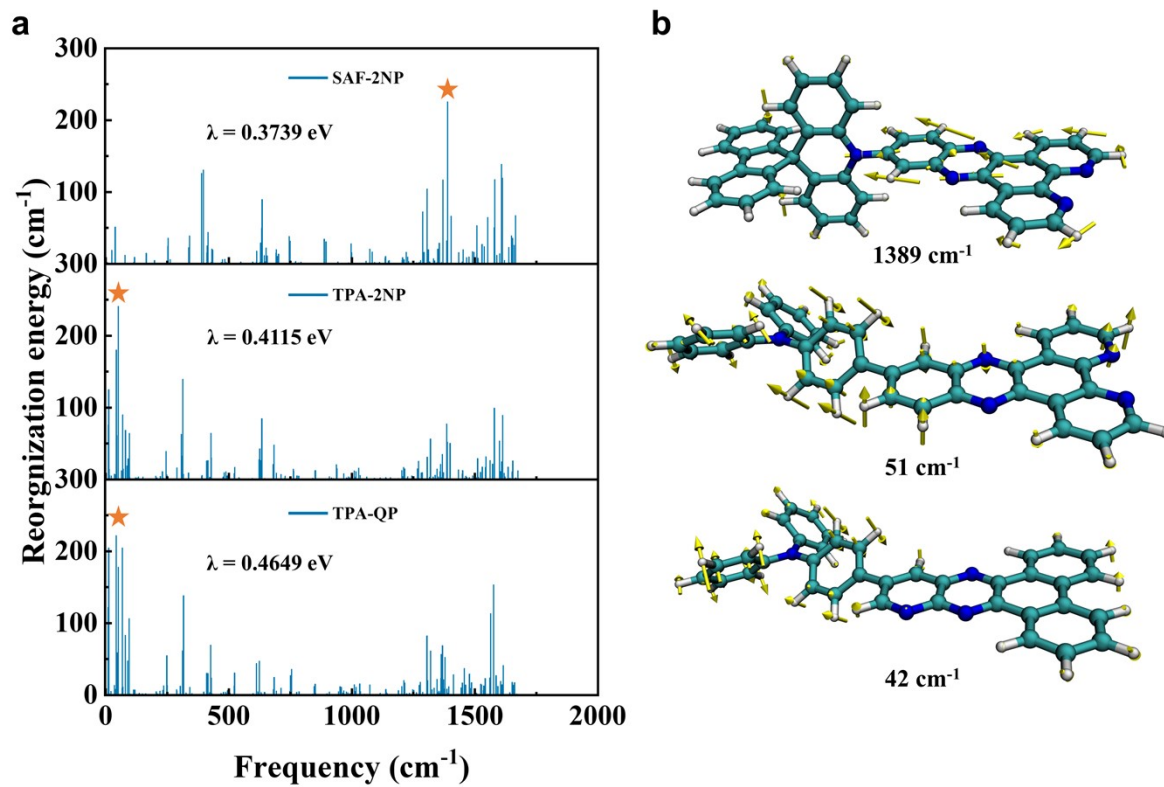
Figure S6. Reorganization energy (λ) versus normal mode frequency (a) and dominant vibrational modes (b) of SAF-2NP, TPA-2NP and TPA-QP.
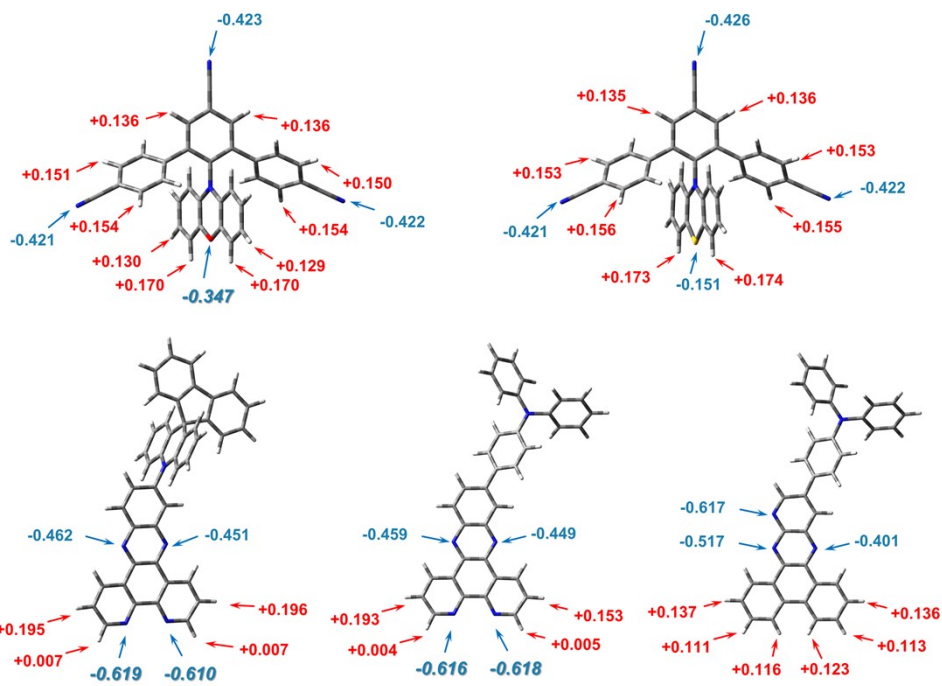
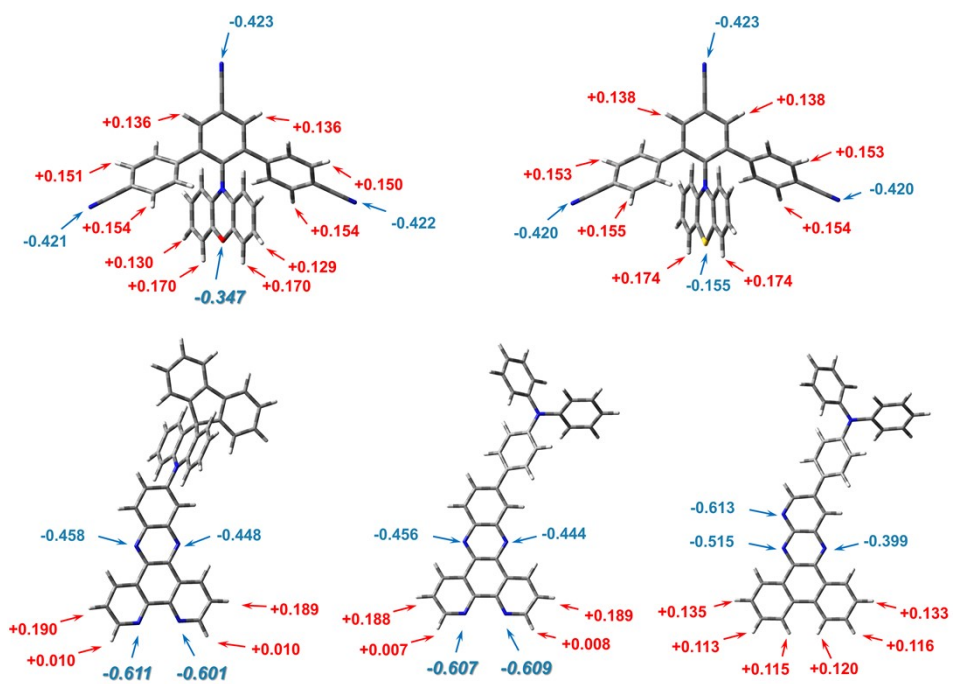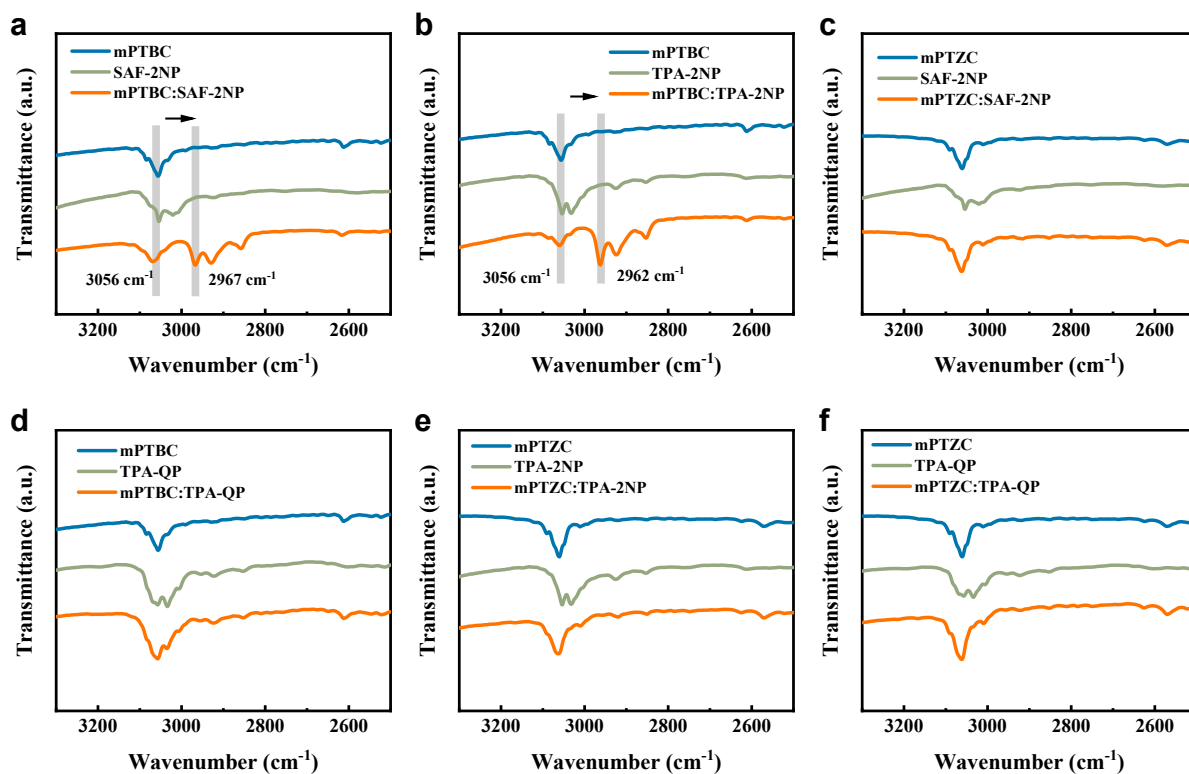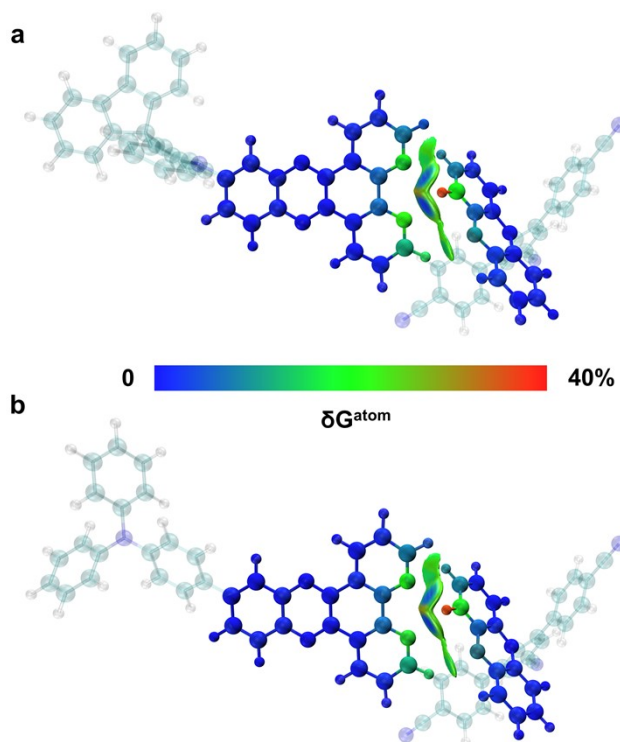**Figure S7.** Key atomic charges fitting through electrostatic potential.

Figure S8. Atomic charges fitted using restrained electrostatic potential (RESP).

Figure S9. Solid film Fourier transform infrared (FT-IR) spectra of six exciplexes (weight ratios = 9:1) and their constituting materials.

Figure S10. Atom contribution to the (a) mPTBC:SAF-2NP and (b) mPTBC:TPA-2NP intermolecular interaction (pure red denotes 40% contribution).
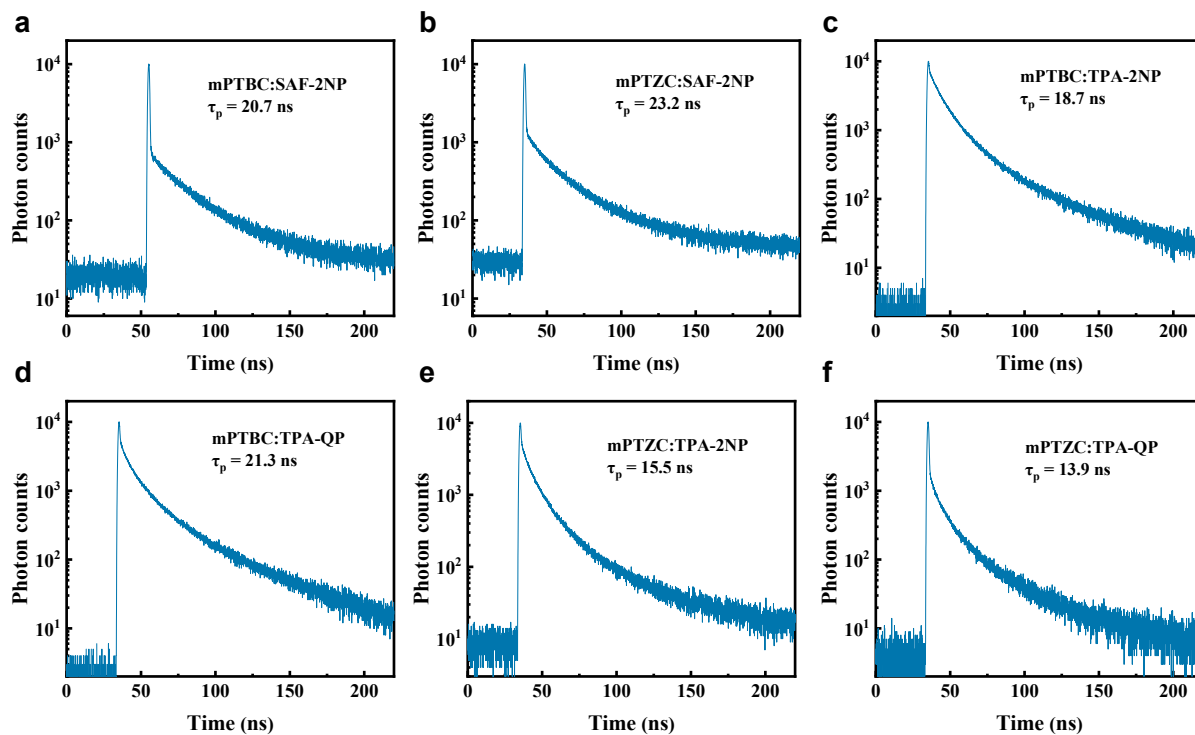
Transient PL properties and rate constants

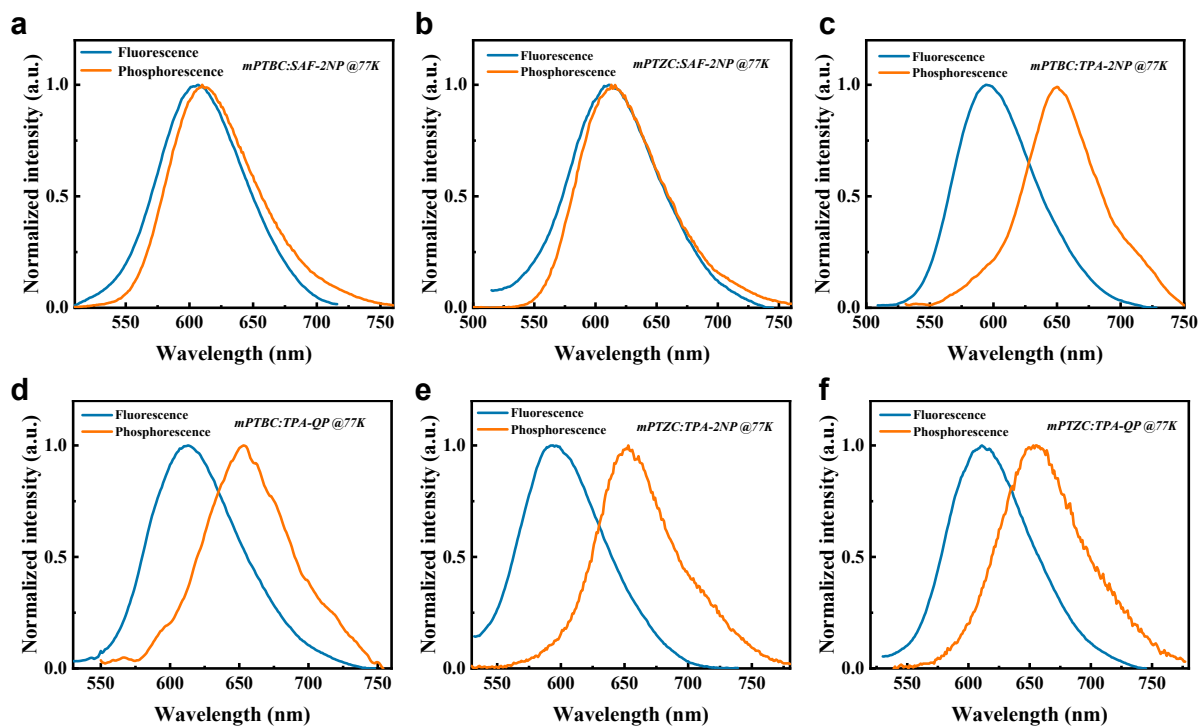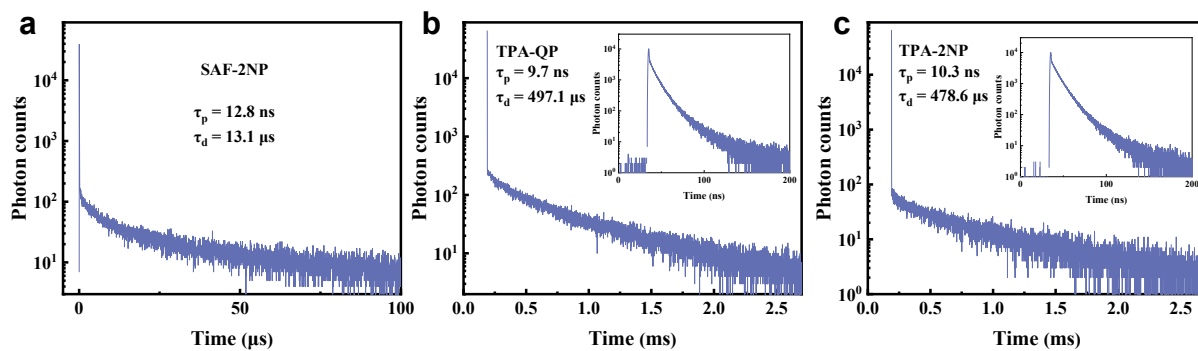**Figure S11.** Solid-state prompt decay curves of the six exciplexes.

Figure S12. Solid-state fluorescence and phosphorescence spectra of films of the six exciplexes measured at 77K.
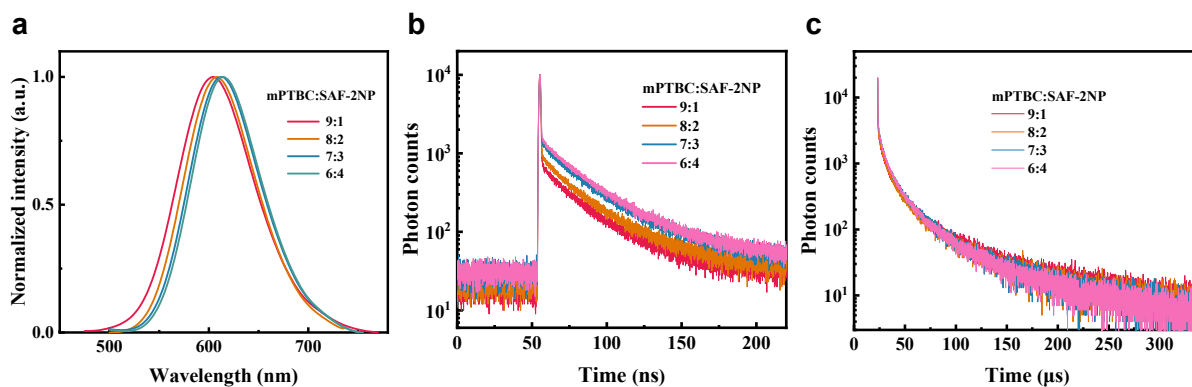
Figure S13. Transient decay curves of SAF-2NP, TPA-2NP and TPA-QP (10 wt% doped in CBP).

Table S2. Summary of photophysical properties of mPTBC:SAF-2NP with acceptor concentration from 10% to 40%.

| Weight ratio	λ_{PL} [nm]	Φ_{PL} [%]	τ_p [ns]	τ_d [μs]	k_f [10^6 s^{-1}]	k_{ISC} [10^7 s^{-1}]	k_{RISC} [10^5 s^{-1}]	k_{nr} [10^6 s^{-1}]
9:1	604	84.1	20.7	22.3	10.50	3.57	1.74	1.98
8:2	608	83.1	22.3	20.1	10.14	3.25	1.83	2.06
7:3	612	78.2	24.9	19.1	8.36	2.93	1.97	2.33
6:4	614	72.3	25.9	18.5	7.09	2.86	2.13	2.72

Figure S14. PL spectra (a), prompt (b) and delayed (c) fluorescence curves of mPTBC:SAF-2NP solid films with different concentrations.

Table S3. Summary of photophysical properties of mPTZC:SAF-2NP, mPTBC:TPA-2NP, mPTBC:TPA-QP, mPTZC:TPA-2NP and mPTZC:TPA-QP with different acceptor concentrations.

| Emitter	Weight ratio [%]	Φ_{PL} [%]	τ_p [ns]	τ_d [µs]	k_f [10^6 s^{-1}]	k_{ISC} [10^7 s^{-1}]	k_{RISC} [10^5 s^{-1}]	k_{nr} [10^6 s^{-1}]
mPTZC:SAF-2NP	9:1	67.5%	23.2	17.5	5.82	3.43	2.86	2.80
	8:2	60.7%	26.3	15.2	4.40	3.05	3.45	2.85
mPTBC:TPA-2NP	9:1	63.6%	18.7	65.2	7.04	4.18	0.71	4.22
	8:2	44.5%	17.6	58.3	5.43	4.46	0.80	6.77
mPTBC:TPA-QP	9:1	40.9%	21.3	59.6	3.12	3.92	1.03	4.51
	8:2	28.2%	16.8	59.2	2.50	5.06	1.14	6.36
mPTZC:TPA-2NP	9:1	32.6%	15.5	77.7	2.58	5.65	1.05	5.34
	8:2	20.3%	14.6	74.4	1.68	6.01	1.11	6.60
mPTZC:TPA-QP	9:1	25.3%	13.9	62.6	2.25	6.29	1.29	6.65
	8:2	16.7%	13.1	66.1	2.33	6.23	0.83	11.63
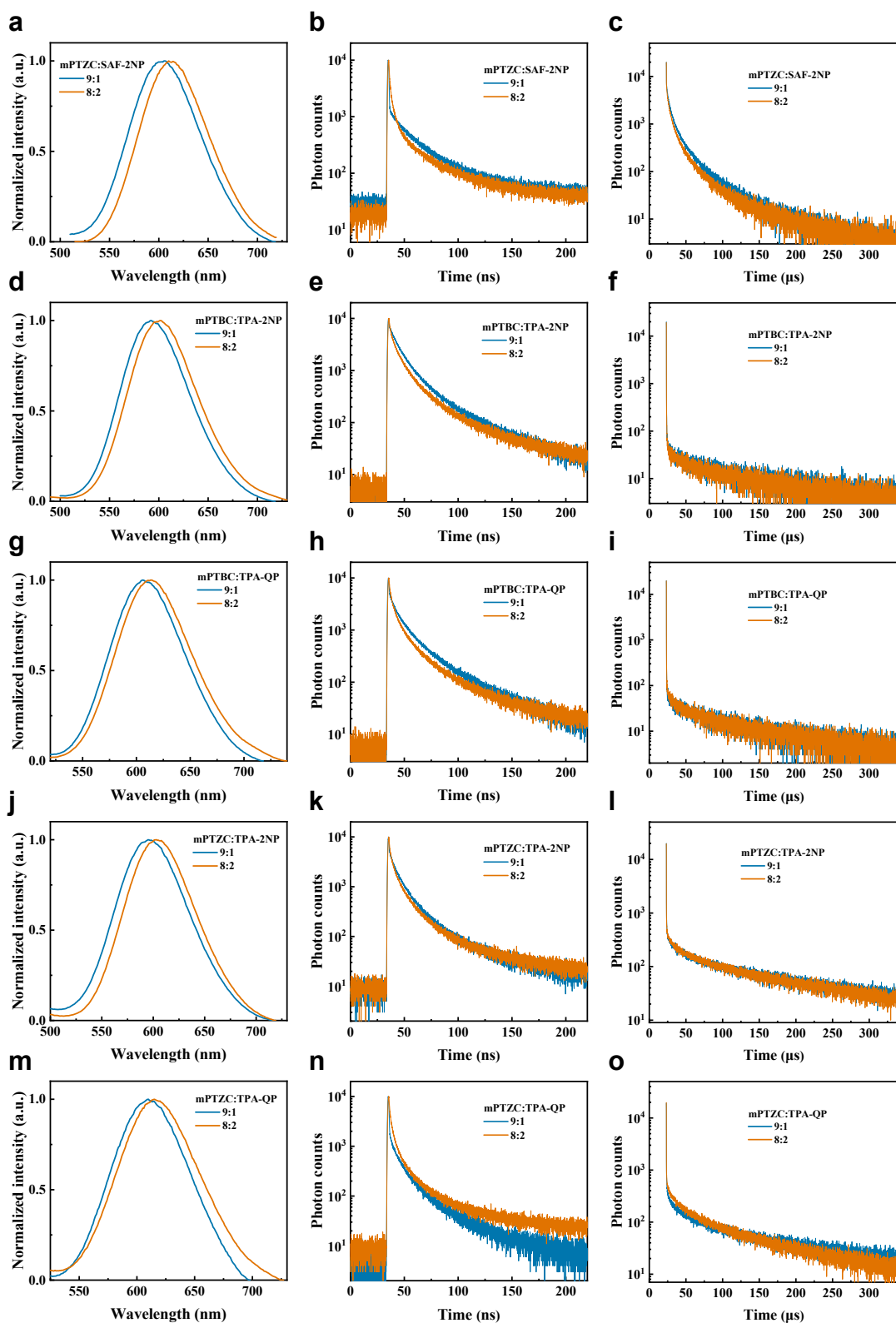
Figure S15. PL spectra, transient decay curves of nanosecond and microsecond scale of mPTZC:SAF-2NP (a-c), mPTBC:TPA-2NP (d-f), mPTBC:TPA-QP (g-i), mPTZC:TPA-2NP (j-l) and mPTZC:TPA-QP (m-o) blend films.

Crystallographic characterization
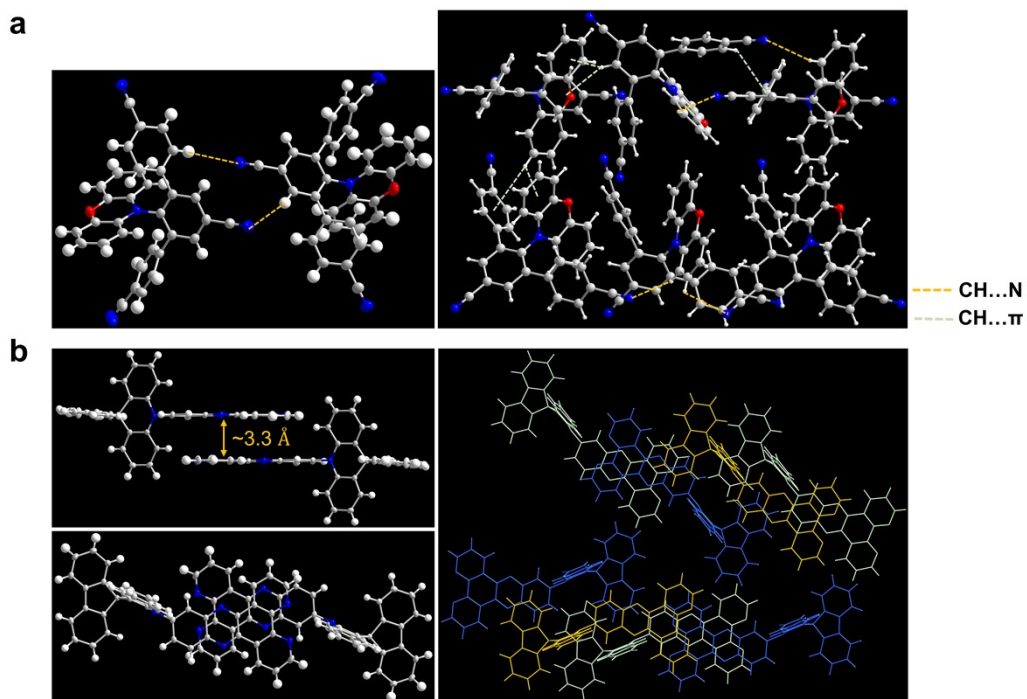
Figure S16. Crystal structures and packing modes of mPTBC (a) and SAF-2NP (b), (right: each color represents a different layer; solvent molecules are hidden for better clarity).
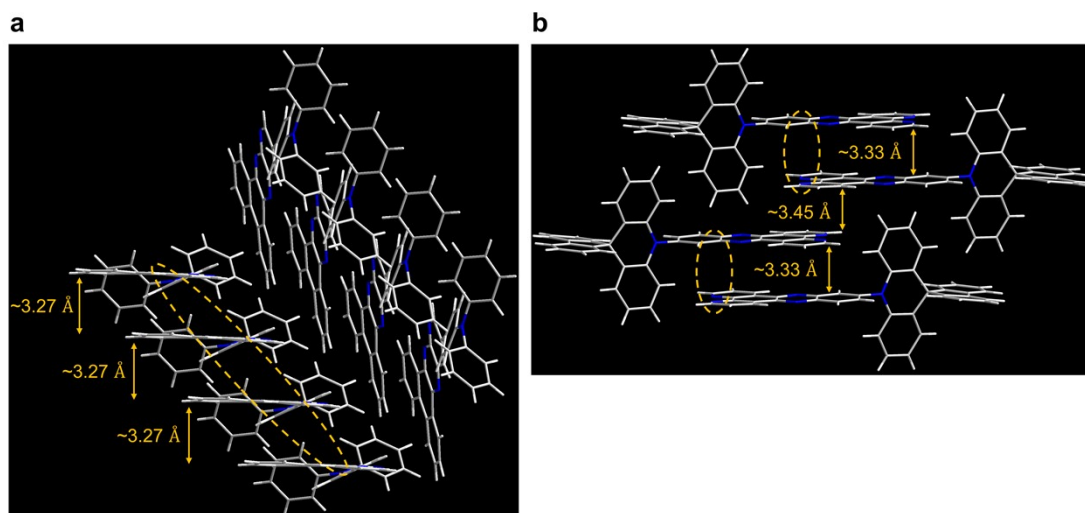
Figure S17. Packing modes of TPA-QP (a) and SAF-2NP (b) obtained from single crystals (solvent molecules are hidden for better clarity).

Table S4.

Crystallographic data.

|	mPTBC	SAF-2NP
Empirical formula	$C_{33}H_{18}N_4O$	$C_{47}H_{35}N_5O$
Formula weight	486.51	685.80
Temperature [K]	150(2)	150(2)
Crystal system	monoclinic	monoclinic
Space group (number)	$P2_1/c$ (14)	$P2_1/n$ (14)
a [Å]	16.7347(4)	8.5144(8)
b [Å]	32.9396(6)	25.961(3)
c [Å]	9.1702(2)	16.1272(16)
α [°]	90	90
β [°]	94.685(2)	101.375(5)
γ [°]	90	90
Volume [Å^3]	5038.04(19)	3494.8(6)
Z	8	4
ρ_{calc} [gcm^{-3}]	1.283	1.303
μ [mm^{-1}]	0.631	0.620
$F(000)$	2016	1440
Crystal size [mm^3]	0.2×0.1×0.1	0.1×0.1×0.1
Crystal colour	colourless	orange
Crystal shape	block	block
Radiation	CuK_α (λ=1.54178 Å)	CuK_α (λ=1.54178 Å)
2θ range [°]	5.30 to 136.57 (0.83 Å)	6.55 to 136.88 (0.83 Å)
Index ranges	$-16 \leq h \leq 20$	$-10 \leq h \leq 10$
	$-39 \leq k \leq 39$	$-31 \leq k \leq 31$
	$-11 \leq l \leq 11$	$-18 \leq l \leq 19$
Reflections collected	43591	37133
Independent reflections	9221	6377
	$R_{int} = 0.0679$	$R_{int} = 0.0547$
	$R_{sigma} = 0.0484$	$R_{sigma} = 0.0336$
Completeness to	100.0 %	99.8 %
θ = 67.679°		
Data / Restraints / Parameters	9221/0/686	6377/0/481
Goodness-of-fit on F^2	0.964	1.038
Final R indexes	$R_1 = 0.0458$	$R_1 = 0.0414$
[$I{\geq}2\sigma(I)$]	w$R_2 = 0.1134$	w$R_2 = 0.1083$
Final R indexes	$R_1 = 0.0743$	$R_1 = 0.0493$
[all data]	w$R_2 = 0.1300$	w$R_2 = 0.1144$
Largest peak/hole [eÅ^{-3}]	0.28/-0.29	0.28/-0.26
Extinction coefficient	0.00097(9)	0.00052(9)

Device characterization
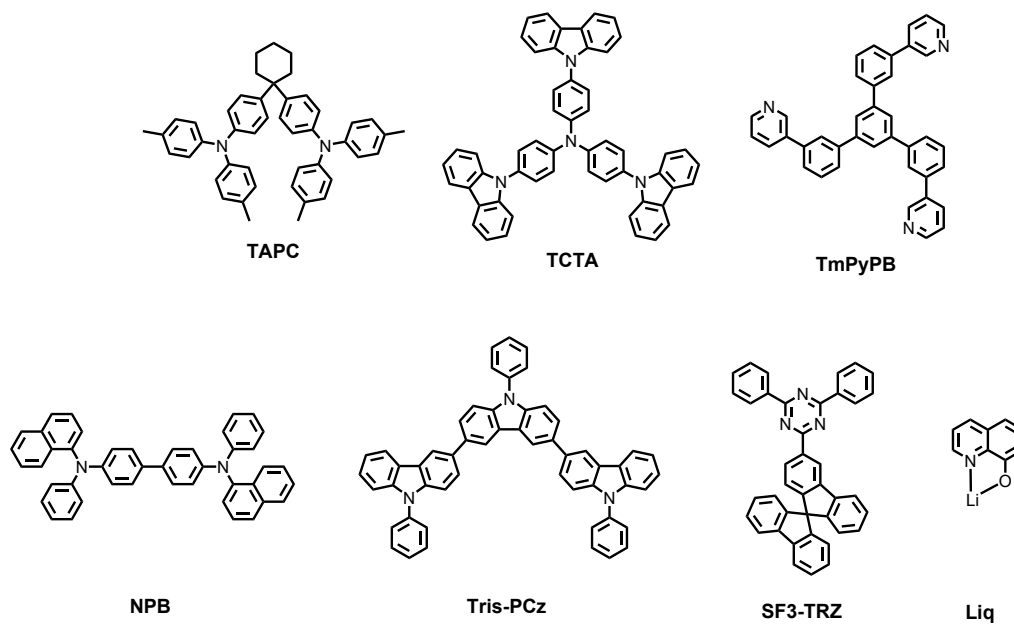
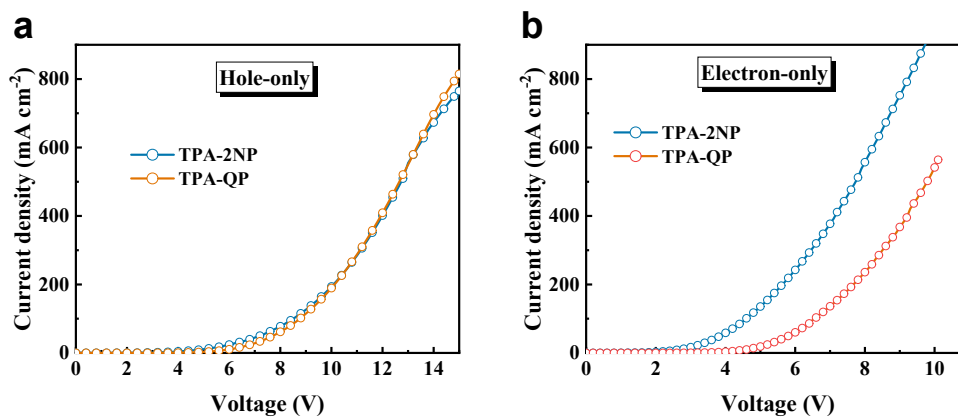**Figure S18.** Chemical structures of functional layer materials used in the electroluminescence devices.
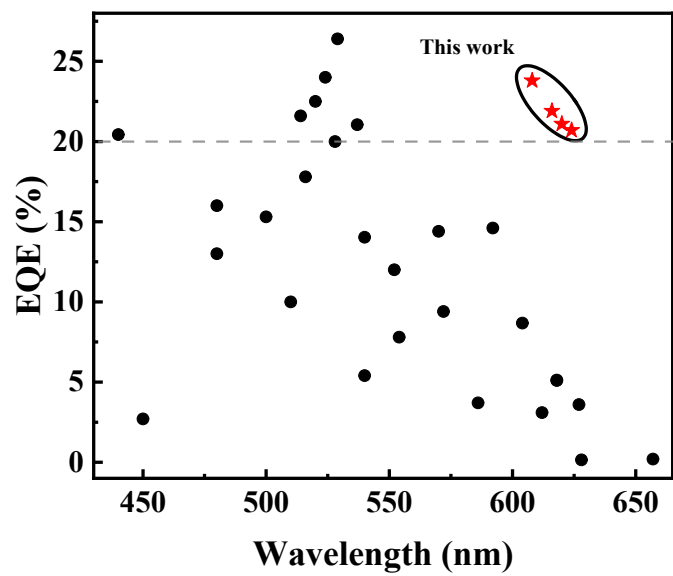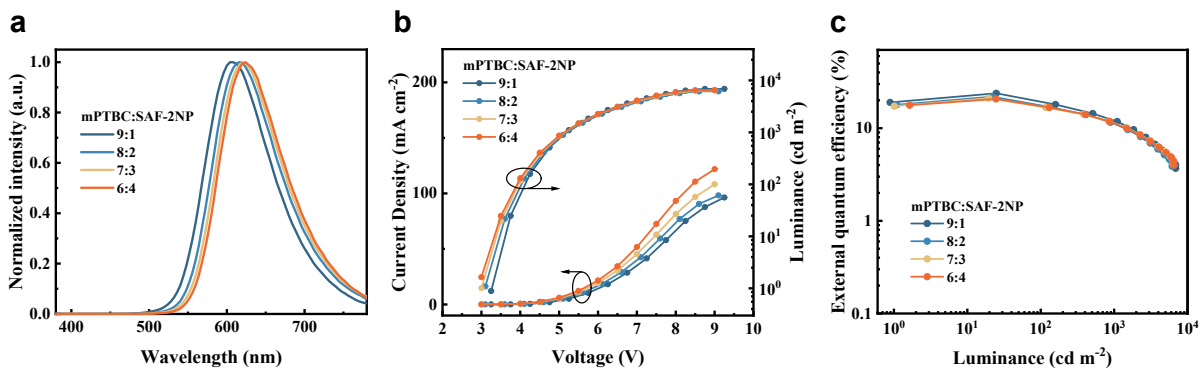

**Figure S19.** Current density-voltage characteristic of (a) hole-only and (b) electron-only devices based on TPA-2NP and TPA-QP.

Figure S20. EQE vs. wavelength plot of representative OLEDs based on exciplex emitters.
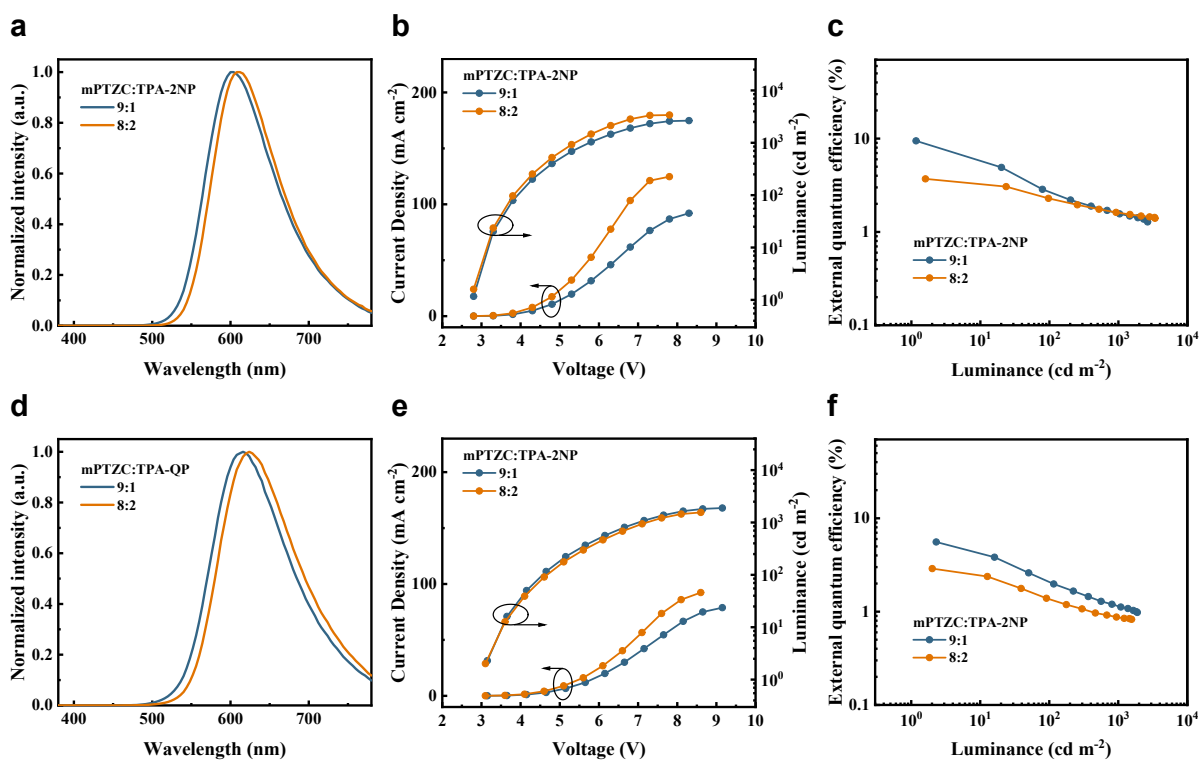
Figure S21. Electroluminescence spectra (a), luminance-voltage-current density curves (b) and EQE-luminance plot (c) of mPTBC:SAF-2NP-based devices with different D:A weight ratios.
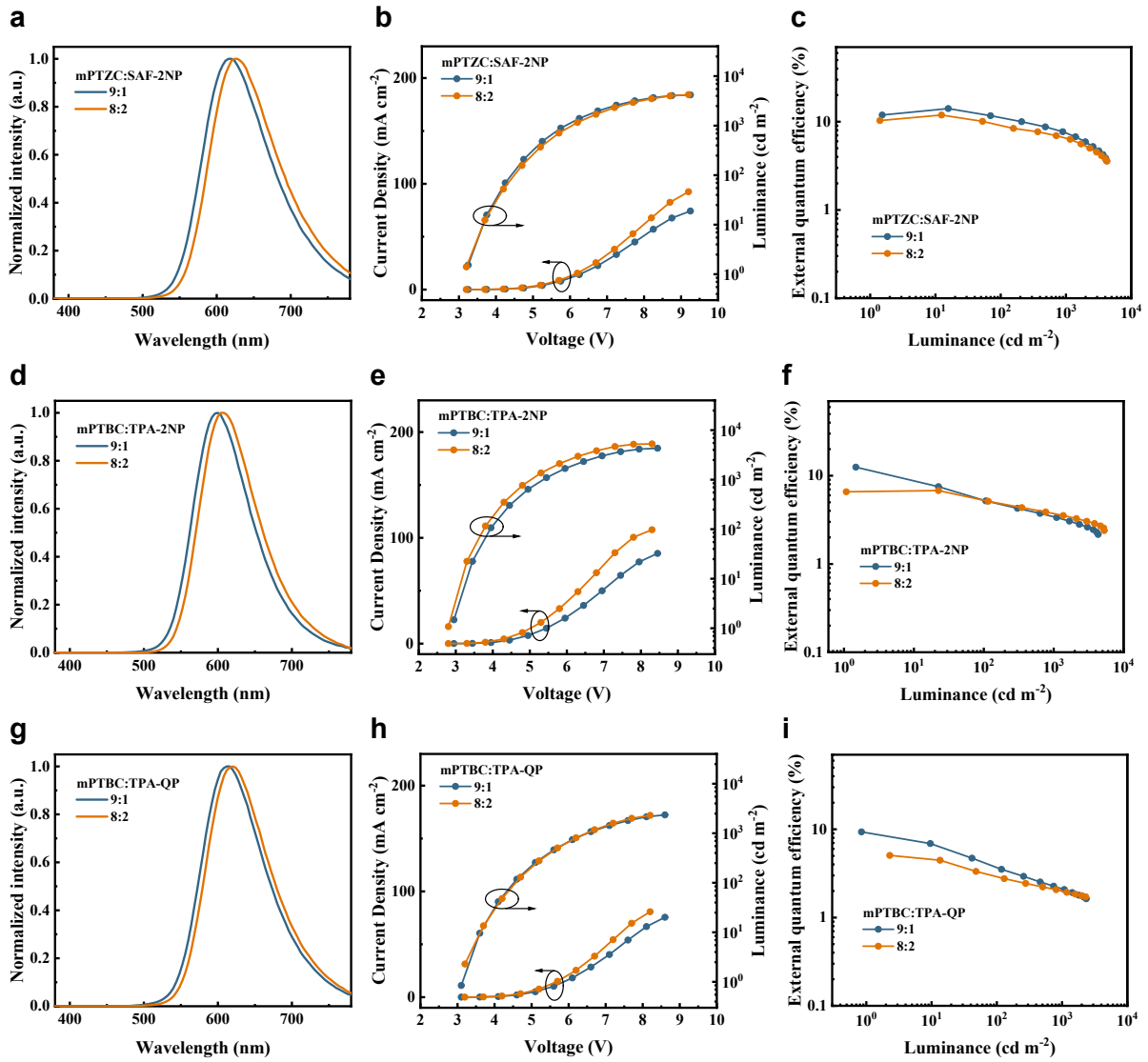
Figure S22. OLED performances using mPTZC:SAF-2NP (a-c), mPTBC:TPA-2NP (d-f) and mPTBC:TPA-QP (g-i) as emitters with different D:A weight ratios.

Figure S23. OLED performances using mPTZC:TPA-2NP (a-c) and mPTZC:TPA-QP (d-f) as emitters with different D:A weight ratios.

Table S5. Summary of EL performance based on mPTZC:SAF-2NP, mPTBC:TPA-2NP, mPTBC:TPA-QP, mPTZC:TPA-2NP and mPTZC:TPA-QP with increased acceptor ratio.

| Emitter	Weight ratio	V_{on}[a] [V]	λ_{EL}[b] [nm]	Maximum CE/PE/EQE [cd A^{-1}/lm W^{-1}/%]	EQE$_{max}$ drop rate[c] [%]	CIE[b] [x,y]
mPTZC:SAF-2NP	8:2	3.2	624	13.3/11.3/11.9	15.6	(0.63, 0.37)
mPTBC:TPA-2NP	8:2	2.8	608	11.9/12.2/6.79	45.7	(0.59, 0.41)
mPTBC:TPA-QP	8:2	3.1	620	6.52/6.4/5.06	45.8	(0.61, 0.39)
mPTZC:TPA-2NP	8:2	2.8	612	5.23/5.86/3.7	56.7	(0.60, 0.40)
mPTZC:TPA-QP	8:2	3.0	624	3.19/3.23/2.89	48.2	(0.62, 0.38)

[a] Driving voltage at 1 cd m^{-2}. [b] At 100 cd m^{-2}. [c] The EQE$_{max}$ drop rate from D:A = 9:1 to 8:2.

**Table S6.** Representative exciplex emitters and their EL properties in Figure S18.

Exciplex emitter	λ_max [nm]	EQE_max [%]	CIE [x,y]	Ref.
mPTBC:SAF-2NP (9:1)	**608**	**23.8**	**(0.58, 0.42)**	
mPTBC:SAF-2NP (8:2)	**616**	**21.9**	**(0.61, 0.39)**	**This work**
mPTBC:SAF-2NP (7:3)	**620**	**21.1**	**(0.62, 0.38)**	
mPTBC:SAF-2NP (6:4)	**624**	**20.7**	**(0.63, 0.37)**	
m-MTDATA:t-Bu-PBD	540	5.4	--	[4]
m-MTDATA:3TPYMB	510	10.0	--	
NPB:TPBi	450	2.7	(0.15, 0.13)	[5]
NPNPB/PO-T2T	657	0.2	(0.64,0.36)	[6]
2d:TAPC	540	14.03	--	[7]
CDBP:POT2T	480	13.0	(0.17, 0.29)	[8]
TAPC/TmPyTZ	552	12.02	(0.432, 0.548)	[9]
TCzTrz:DMAC-DPS	500	15.3	(0.25, 0.46)	[10]
MAC:PO-T2T	516	17.8	(0.31, 0.55)	[11]
pCNBCzoCF3/m-MTDATA	572	9.4	(0.44, 0.44)	[12]
DPSTPA:CzDBA	592	14.6	(0.53, 0.46)	[13]
mCP:PO-T2T	480	16	(0.16, 0.28)	
TSBPA:PO-T2T	528	20	(0.33, 0.57)	[14]
DNTPD:PO-T2T	628	0.15	(0.60, 0.39)	
TPA-3:9PhFDPhTz/PO-T2T	524	24	--	[15]
BCzPh:CN-T2T	537	21.05	(0.36, 0.56)	[16]
BCzPh:CN-T2T	529	26.4	(0.33, 0.56)	[17]
PVK:PO-T2T:mCP	514	21.6	(0.26, 0.51)	[18]
TCTA:TRZSFX	520	22.5	(0.35, 0.60)	[19]
DBFDPO-MnBr2:Bepp2	604	8.68	--	[20]
B2PyMPM:Ir-817	612	3.1	(0.58,0.42)	[21]
TCTA:3P-T2T	554	7.8	(0.40, 0.55)	[22]
TAPC/PO-T2T	586	3.7	(0.51, 0.48)	[23]
TAPC:3P-T2T tandem	570	14.4	--	[24]
CPTBF:m-QCN (2:1)	618	5.12	--	[25]
CPTBF:m-QCN (1:1)	627	3.6	--	
CzSiTrz	440	20.43	(0.157,0.076)	[26]
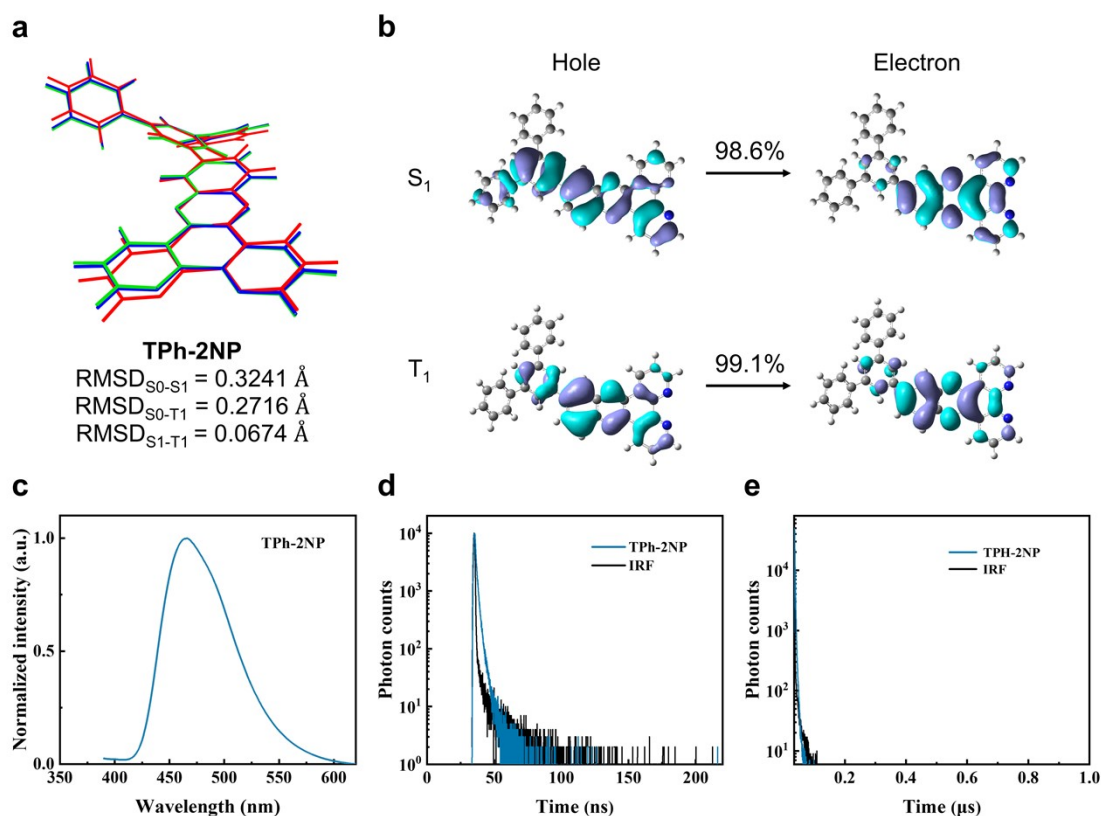
Figure S24. Theoretical calculations and photophysical properties of TPh-2NP. (a) Optimized S0, S1, and T1 geometries and corresponding RMSD values. (b) Natural transition orbitals of S1 and T1. (c) Steady-state PL spectrum of TPh-2NP neat film. Transient PL decay curves of TPh-2NP measured at the nanosecond (d) and microsecond (e) range.
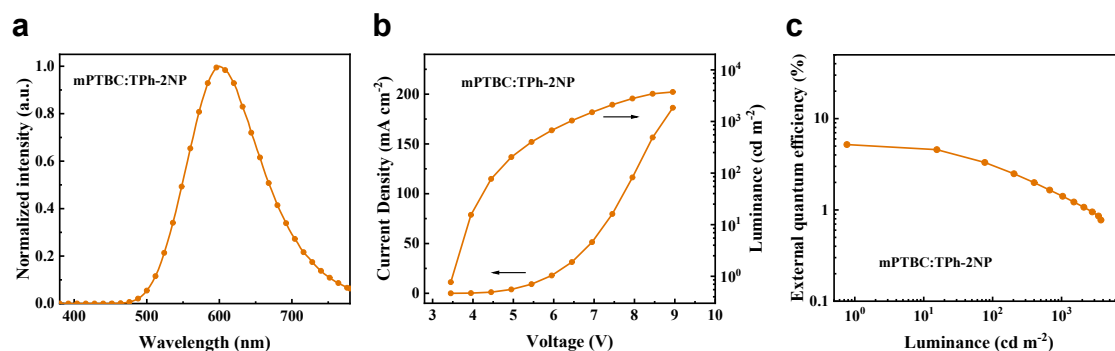
Figure S25. The EL spectrum (a), current density-voltage-luminance curves (b) and EQE-luminance plot (c) of mPTBC:TPh-2NP-based OLEDs. The device structure is ITO/TPAC (35 nm)/TCTA (10 nm)/mPTBC:TPh-2NP (95:5, 20 nm)/TmPyPB (65 nm)/LiF (1 nm)/Al (100 nm).
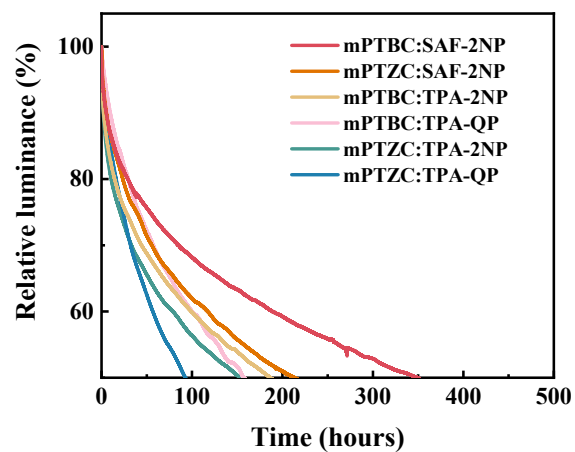
Figure S26. Luminance decay curves of devices based on mPTBC:SAF-2NP, mPTZC:SAF-2NP, mPTBC:TPA-2NP, mPTBC:TPA-QP, mPTZC:TPA-2NP and mPTZC:TPA-QP.
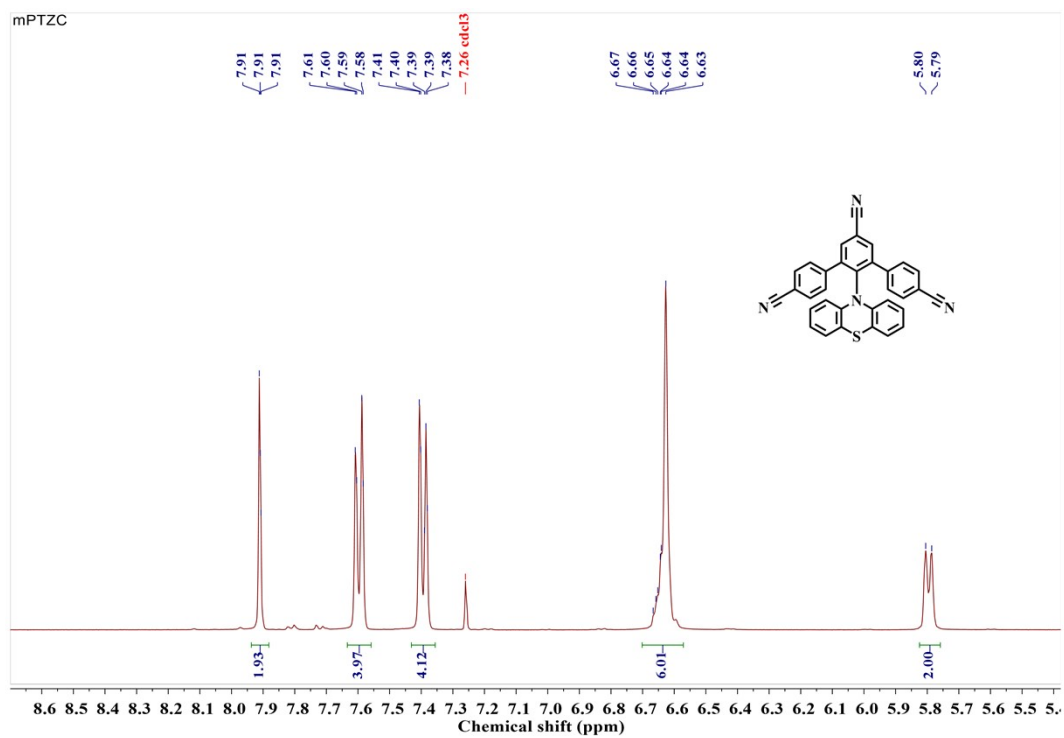
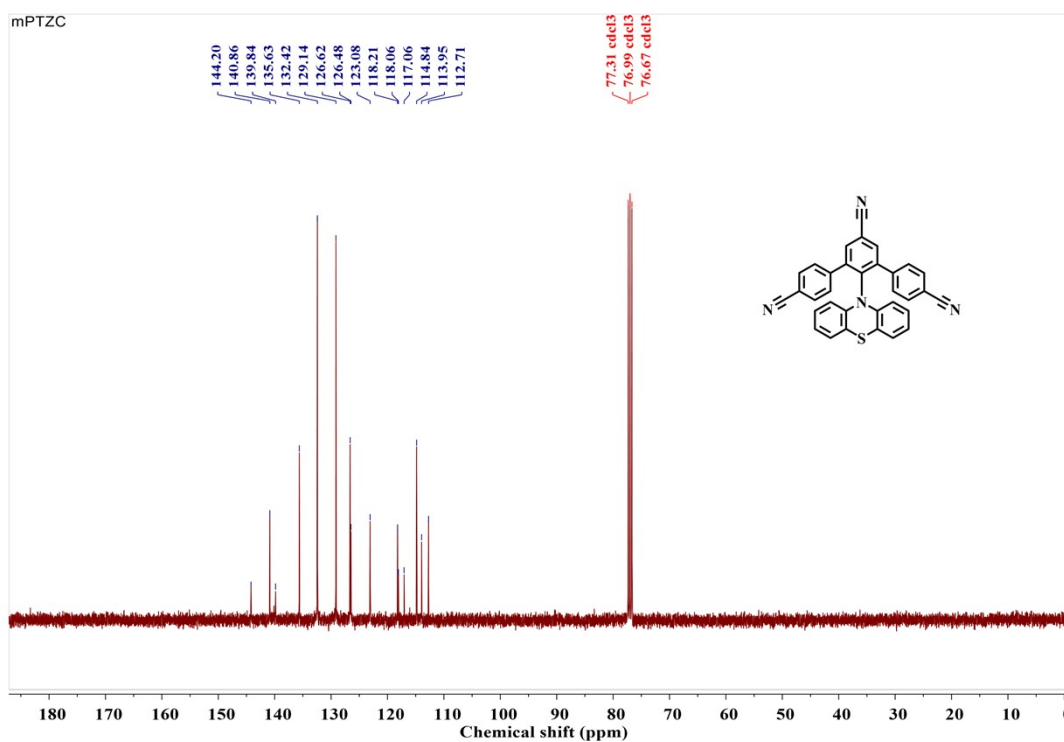# NMR spectra

Figure S27. ^{1}H NMR of mPTZC in CDCl$_3$.

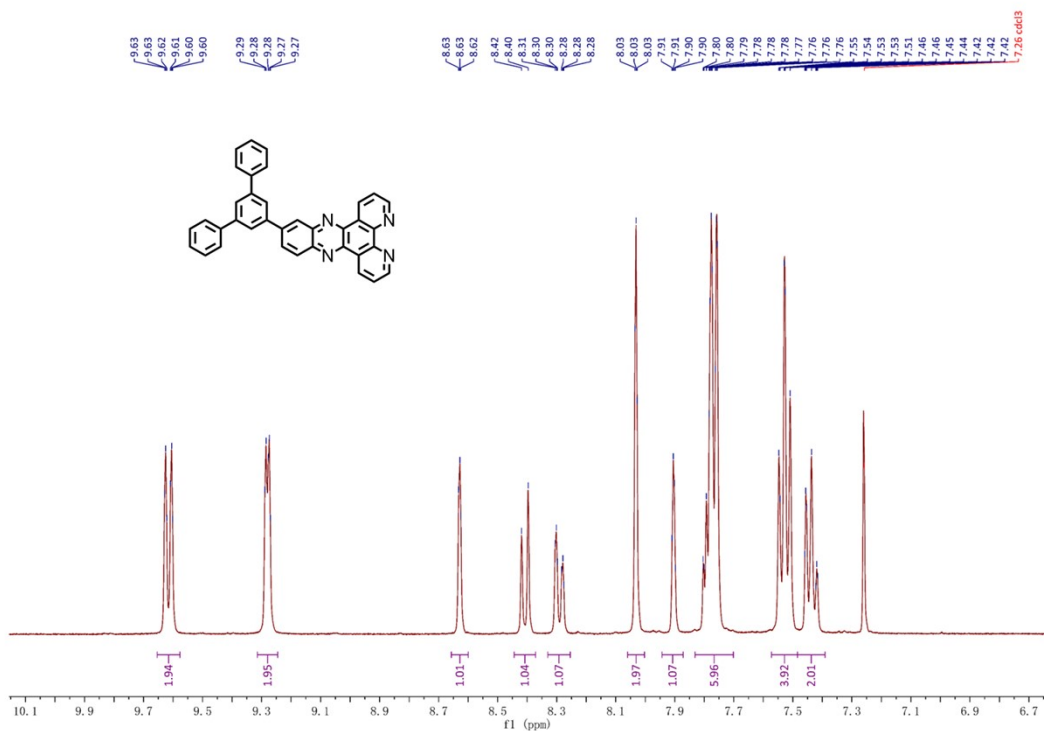**Figure S28.** ^{13}C NMR of mPTZC in CDCl$_3$.

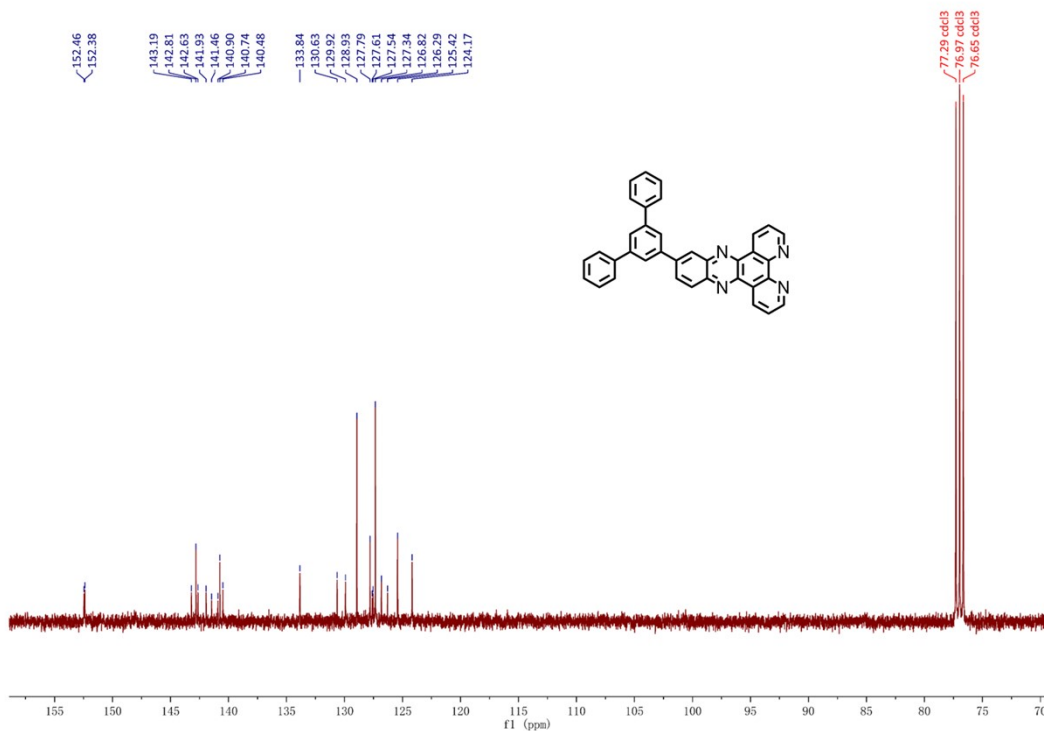**Figure S29.** ^{1}H NMR of TPh-2NP in CDCl$_3$.

Figure S30. ^{13}C NMR of TPh-2NP in CDCl$_3$.

Reference

[1] Y. Wada, H. Nakagawa, S. Matsumoto, Y. Wakisaka, H. Kaji, Nat. Photonics 2020, 14, 643.

[2] D.-Q. Wang, M. Zhang, K. Wang, C.-J. Zheng, Y.-Z. Shi, J.-X. Chen, H. Lin, S.-L. Tao, X.-H. Zhang, Dyes Pigments 2017, 143, 62.

[3] H.-Y. Zhang, H.-Y. Yang, M. Zhang, H. Lin, S.-L. Tao, C.-J. Zheng, X.-H. Zhang, Mater. Horiz. 2022, 9, 2425.

[4] K. Goushi, K. Yoshida, K. Sato, C. Adachi, Nat. Photonics 2012, 6, 253.

[5] V. Jankus, C. Chiang, F. Dias, A. P. Monkman, Adv. Mater. 2013, 25, 1455.

[6] W.-Y. Hung, G.-C. Fang, S.-W. Lin, S.-H. Cheng, K.-T. Wong, T.-Y. Kuo, P.-T. Chou, Sci. Rep. 2014, 4, 5161.

[7] V. Jankus, P. Data, D. Graves, C. McGuinness, J. Santos, M. R. Bryce, F. B. Dias, A. P. Monkman, Adv. Funct. Mater. 2014, 24, 6178.

[8] X. Liu, Z. Chen, J. Qing, W. Zhang, B. Wu, H. L. Tam, F. Zhu, X. Zhang, C. Lee, Adv. Mater. 2015, 27, 7079.

[9] D. Chen, G. Xie, X. Cai, M. Liu, Y. Cao, S. Su, Adv. Mater. 2016, 28, 239.

[10] S. K. Jeon, K. S. Yook, J. Y. Lee, Nanotechnology 2016, 27, 224001.

[11] W. Liu, J.-X. Chen, C.-J. Zheng, K. Wang, D.-Y. Chen, F. Li, Y.-P. Dong, C.-S. Lee, X.-M. Ou, X.-H. Zhang, Adv. Funct. Mater. 2016, 26, 2002.

[12] G. Grybauskaite-Kaminskiene, K. Ivaniuk, G. Bagdziunas, P. Turyk, P. Stakhira, G. Baryshnikov, D. Volyniuk, V. Cherpak, B. Minaev, Z. Hotra, H. Ågren, J. V. Grazulevicius, J. Mater. Chem. C 2018, 6, 1543.

[13] T.-L. Wu, S.-Y. Liao, P.-Y. Huang, Z.-S. Hong, M.-P. Huang, C.-C. Lin, M.-J. Cheng, C.-H. Cheng, ACS Appl. Mater. Interfaces 2019, 11, 19294.

[14] M. Chapran, P. Pander, M. Vasylieva, G. Wiosna-Salyga, J. Ulanski, F. B. Dias, P. Data, ACS Appl. Mater. Interfaces 2019, 11, 13460.

[15] J. Zhao, C. Zheng, Y. Zhou, C. Li, J. Ye, X. Du, W. Li, Z. He, M. Zhang, H. Lin, S. Tao, X. Zhang, Mater. Horiz. 2019, 6, 1425.

[16] M. Wang, Y. Huang, K. Lin, T. Yeh, J. Duan, T. Ko, S. Liu, K. Wong, B. Hu, Adv. Mater. 2019, 31, 1904114.

[17] N. R. Al Amin, K. K. Kesavan, S. Biring, C.-C. Lee, T.-H. Yeh, T.-Y. Ko, S.-W. Liu, K.-T. Wong, ACS Appl. Electron. Mater. 2020, 2, 1011.

[18] P.-L. Zhong, C.-J. Zheng, M. Zhang, J.-W. Zhao, H.-Y. Yang, Z.-Y. He, H. Lin, S.-L. Tao, X.-H. Zhang, Org. Electron. 2020, 76, 105449.

[19] H.-T. Cao, J. Wan, B. Li, H. Zhang, L.-H. Xie, C. Sun, Q.-Y. Feng, W.-J. Yu, W. Huang, Dyes Pigments 2021, 185, 108894.

[20] Y. Qin, P. Tao, L. Gao, P. She, S. Liu, X. Li, F. Li, H. Wang, Q. Zhao, Y. Miao, W. Huang, Adv. Opt. Mater. 2019, 7, 1801160.

[21] M. Zhang, C.-J. Zheng, H.-Y. Zhang, H.-Y. Yang, K. Wang, Y.-Z. Shi, H. Lin, S.-L. Tao, X.-H. Zhang, J. Mater. Chem. C 2022, 10, 15593-15600.

[22] W.-Y. Hung, G.-C. Fang, Y.-C. Chang, T.-Y. Kuo, P.-T. Chou, S.-W. Lin, K.-T. Wong, ACS Appl. Mater. Interfaces 2013, 5, 6826-6831.

[23] W.-Y. Hung, G.-C. Fang, S.-W. Lin, S.-H. Cheng, K.-T. Wong, T.-Y. Kuo, P.-T. Chou, Sci Rep 2014, 4, 5161.

[24] B. Zhao, T. Zhang, B. Chu, W. Li, Z. Su, Y. Luo, R. Li, X. Yan, F. Jin, Y. Gao, H. Wu, Org. Electron. 2015, 17, 15-21.

[25] G. C. Liu, T. H. Huang, H. W. Wang, C. H. Hsu, P. T. Chou, W. Y. Hung, K. T. Wong, Chem. Eur. J. 2023, 29, e202203660.

[26] Z. Zhang, D. Dou, R. Xia, P. Wu, E. Spuling, K. Wang, J. Cao, B. Wei, X. Li, J. Zhang, S. Bräse, Z. Wang, Sci. Adv. 2023, 9, eadf4060.